Temperature Induced Morphological Transitions from Native to Unfolded Aggregated States of Human Serum Albumin

ARTICLE *in* THE JOURNAL OF PHYSICAL CHEMISTRY B · JUNE 2014

Impact Factor: 3.3 · DOI: 10.1021/jp5030944 · Source: PubMed

THE JOURNAL OF PHYSICAL CHEMISTRY B

Article

pubs.acs.org/JPCB

Temperature Induced Morphological Transitions from Native to Unfolded Aggregated States of Human Serum Albumin

Nirmal Kumar Das, Narayani Ghosh, Ajit Prabhakar Kale, Ramakanta Mondal, Uttam Anand, Subhadip Ghosh, Virendra Kumar Tiwari, Manmohan Kapur,* and Saptarshi Mukherjee*

Department of Chemistry, Indian Institute of Science Education and Research Bhopal Indore By-Pass Road, Bhauri, Bhopal 462 066, Madhya Pradesh, India

Supporting Information

ABSTRACT: The circulatory protein, human serum albumin (HSA), is known to have two melting point temperatures, 56 and 62 °C. In this present manuscript, we investigate the interaction of HSA with a synthesized bioactive molecule 3-pyrazolyl 2-pyrazoline (PZ). The sole tryptophan amino acid residue (Trp214) of HSA and PZ forms an excellent FRET pair and has been used to monitor the conformational dynamics in HSA as a function of temperature. Molecular docking studies reveal that the PZ binds to a site which is in the immediate vicinity of Trp214, and such data are also supported by time-resolved FRET studies. Steady-state and time-resolved anisotropy of PZ conclusively proved that the structural and morphological changes in HSA mainly occur beyond its first melting temperature. Although the protein undergoes thermal denaturation at elevated temperatures, the Trp214 gets buried inside the protein scaffolds; this fact has been substantiated by acrylamide quenching studies. Finally, we have used atomic force microscopy to establish that at around 70 °C, HSA undergoes self-assembly to form fibrillar structures. Such an observation may be attributed to the loss of α-helical content of the protein and a subsequent rise in β-sheet structure.

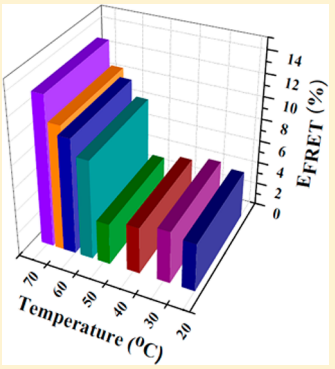

INTRODUCTION

Serum albumins are the most abundant circulatory proteins in blood, constituting nearly 52−60% of plasma and playing a major role as a transporter of various amino acids, drug molecules, fatty acids, hemin, and bilirubin to the target sites.[1,2] In the circulatory system, human serum albumin (HSA) reduces the activity of toxins, affects the pharmacokinetics of many drugs, takes care of the metabolic modifications of some ligands, and also sometimes exhibits pseudoenzymatic activities.[2−8] The protein is composed of a single polypeptide chain having 585 amino acid residues, has an average molecular weight of ∼66 kDa, and also is characterized by low tryptophan (Trp) and high cysteine (Cys) content.[9] HSA adopts a three-dimensional, heart-shaped structure having three homologous domains under physiological conditions.[9] Each of them is again divided into two subdomains A and B that consist of 4 and 6 α-helices, respectively.[1,9] The secondary structure of HSA consists of 17 disulfide bridges and about 67% α-helix having six turns.[10] He and Carter showed that the two halves of HSA form a 10 Å wide and 12 Å deep crevice.[9] A single tryptophan (Trp) residue[1,2] at the position 214 of the amino acid sequence (Trp214) makes it very unique and this property enables HSA to be studied extensively making use of the intrinsic fluorescence of this Trp214. HSA is a very efficient protein for binding and transporting drugs or bioactive molecules to their target sites. There are two binding sites of HSA: (i) subdomain IIA (commonly referred to as Sudlow's site I, warfarin-binding site) and (ii) subdomain IIIA (commonly referred to as Sudlow's site II, indole/benzodiazepine site).[11] Both hydrophobic and electrostatic interactions play major roles for bindings of drugs or bioactive molecules to HSA. Bulky heterocyclic molecules having centrally delocalized negative charges preferably bind to the hydrophobic pocket of domain IIA, i.e., Sudlow's site I.[12,13] Also, theoretical approaches using Lamarckian genetic algorithm (LGA) based molecular docking studies provide us with an idea of binding characteristics of a small molecule with a biomacromolecule.[14−17]

The topic of unfolding/denaturation, i.e., the structural changes of serum albumins brought in by chemical denaturants such as surfactants, drugs, salts, and also by physical denaturants like changes in pH and temperature, has been well-documented.[18−31] Temperature induced conformational changes have also been studied by various methods.[32−35] Flora et al. have investigated the thermal denaturation of HSA and shown that it also takes place in a sequential manner.[35] According to their opinion, at first domain II starts to denature at 56 °C followed by domain I at 62 °C. These two temperatures are commonly referred to as the melting point-1 (T_{m1}) and melting point-2 (T_{m2}), respectively of HSA.[35] According to G. A. Picó, the thermal denaturation process of serum albumins occurs via the Eyring and Lumry model: native

Received: March 28, 2014
Revised: June 10, 2014

   dx.doi.org/10.1021/jp5030944 | J. Phys. Chem. B XXXX, XXX, XXX−XXX

↔ unfolded (reversible) → unfolded (irreversible).[36] He further opined that for temperatures less than 74 °C, the rate of the irreversible process is very slow.[36] Using differential scanning calorimetry (DSC), G. A. Picó also concluded that the thermal conformational changes follow a sequential transition.[36] Pal and co-workers have exhibited that the hydrodynamic radius of HSA increases four times at 75 °C using dynamic light scattering (DLS) experiments.[37] They also studied the thermal unfolding and refolding of HSA and suggested that the protein undergoes both reversible and irreversible folding and refolding, depending upon the experimental conditions.[37] Takeda and co-workers proved by circular dichroism (CD) spectroscopy that with increasing temperature the helical structures of another homologous protein, bovine serum albumin (BSA), are destroyed; more β-sheets and random structures are formed.[38] They also opined that after 65 °C, more β-sheet structures are formed that correlate with the generation of aggregation of protein.[38]

The bioactive molecule, 3-pyrazolyl 2-pyrazoline (PZ) (Scheme 1), was synthesized by following the protocol as

Scheme 1. Structure of PZ

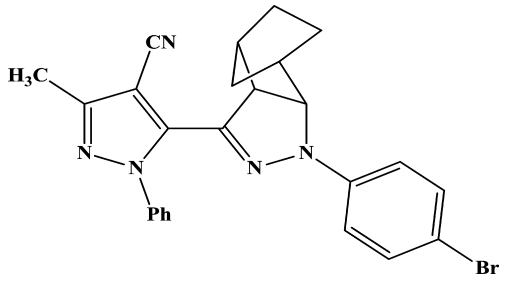

described by Bhattacharya and co-workers.[39] 2-Pyrazoline derivatives constitute a class of compound of pharmaceutical importance as they have inherent antidiabetic, anesthetic, analgesic, and glutamate transport sensor properties.[40] Bhattacharya and co-workers reported earlier that PZ serves as a good fluorescence resonance energy transfer (FRET) pair of Trp214 in HSA and it binds in the close vicinity of this amino acid residue.[41] Hence, this novel bioactive molecule having fluorescent properties is of immense importance for investigations of physiological activities in living systems. FRET is a phenomenon that describes the energy transfer via nonradiative pathway between a donor fluorescent molecule in the excited state and an acceptor fluorophore in the ground state.[42] According to Förster, the efficiency of energy transfer depends upon the extent of overlap between the emission spectra of the donor and absorption spectra of the acceptor, quantum yield of donor molecule, relative dipole orientation of donor and acceptor fluorophores molecules and molar extinctions coefficient of acceptor fluorophores and also distances between donor and acceptor fluorophores. FRET, being a distance dependent phenomenon is sometimes referred to as "biological ruler".[42]

Our present study is focused on the generation of different temperature dependent unfolded states of HSA and also probing the microenvironment in an around the Trp214 residue and the added bioactive fluorescent molecule, PZ. Using steady-state and time-resolved fluorescence techniques, we have concluded that the interactions of PZ with the protein, HSA, are a function of temperature. The conformational changes in HSA brought in by increasing temperature were monitored by FRET studies. We observed that with a rise in temperature, Trp214 gets buried inside the protein matrix and experiences a more hydrophobic environment which was supported by our acrylamide quenching data. Also, using atomic force microscopy (AFM), we have concluded that HSA starts to form aggregates at elevated temperatures; the process of aggregation gets initiated at 56 °C, and interestingly, at 70 °C, it forms aggregated fibrils.

EXPERIMENTAL SECTION

(a). Materials. HSA, essentially fatty acid free and globulin free (A5843, CAS, 70024-90-7) and acrylamide (A9099, CAS, 79-06-1) were purchased from Sigma-Aldrich Co., St. Louis, MO. All solutions were prepared in 50 mM Tris-HCl buffer, pH = 7.4. The final protein concentration was adjusted to 10 μM using absorption values for steady-state and lifetime measurements. The concentration of the protein was determined spectrophotometrically using ε_{280} = 44 000.[21] 3-Pyrazolyl-2-pyrazoline derivative, 5-((3a*S*,7a*R*)-1-(4-bromophenyl)-3a,4,5,6,7,7a-hexahydro-1*H*-4,7-methano-indazol-3-yl)-3-methyl-1-phenyl-1*H*-pyrazole-4-carbonitrile (PZ) (Scheme 1) was synthesized using the method described earlier.[39] Please see Supporting Information SI-1 for the ^{1}H NMR, ^{13}C NMR, and high resolution mass data. For temperature dependent studies, the samples were incubated for 1 h at a particular temperature before carrying out the spectroscopic experiments. To confirm whether PZ undergoes any conformational change(s) due to an increase in temperature, we had carried out a variable temperature NMR study. From the spectra (Supporting Information SI-1), it can be concluded that the structural integrity of PZ remains fully intact as the coupling constants remain unchanged thereby proving that the probe (PZ) can be monitored by all spectroscopic techniques within the temperature window used in this present study.

(b). Steady-State Measurements. Steady-state absorption measurements were carried out in a PerkinElmer UV−vis Spectrophotometer, Lambda-25. All the steady-state fluorescence data were recorded on a HORIBA JOBIN YVON, FLUOROLOG 3-111. The fluorescence spectra were measured with a quartz cuvette of 10 mm path length. HSA was excited at 295 nm in order to minimize the contribution from tyrosine. The fluorescence emission was collected from 305 to 580 nm with an integration time of 0.1 s. On the other hand, PZ was excited at 395 nm and fluorescence emission was collected from 405 to 650 nm with the same integration time. The emission and the excitation slits were kept at 2 and 1 nm, respectively, for monitoring both Trp214 and PZ. The concentration of PZ was kept very low (∼10 μM) so as to minimize the contribution from inner filter effects.

(c). Time-Resolved Fluorescence Measurements. For lifetime measurements, the samples were excited at 295 nm (for monitoring Trp) using a picosecond diode (IBH-NanoLED source N-295) and at 375 nm (for monitoring PZ) using a picosecond diode (IBH-NanoLED source N-375). The emission was collected at magic angle polarization using a Hamamatsu MCP Photomultiplier (Model R-3809U-50). The time-correlated single photon counting (TCSPC) setup consists of an Ortec 9327 pico-timing amplifier. The data was collected with a PCI-6602 interface card as a multichannel analyzer. The typical full width at half maximum of the system response was about 790 and 805 ps for N-295 and N-375, respectively.

dx.doi.org/10.1021/jp5030944 | J. Phys. Chem. B XXXX, XXX, XXX−XXX

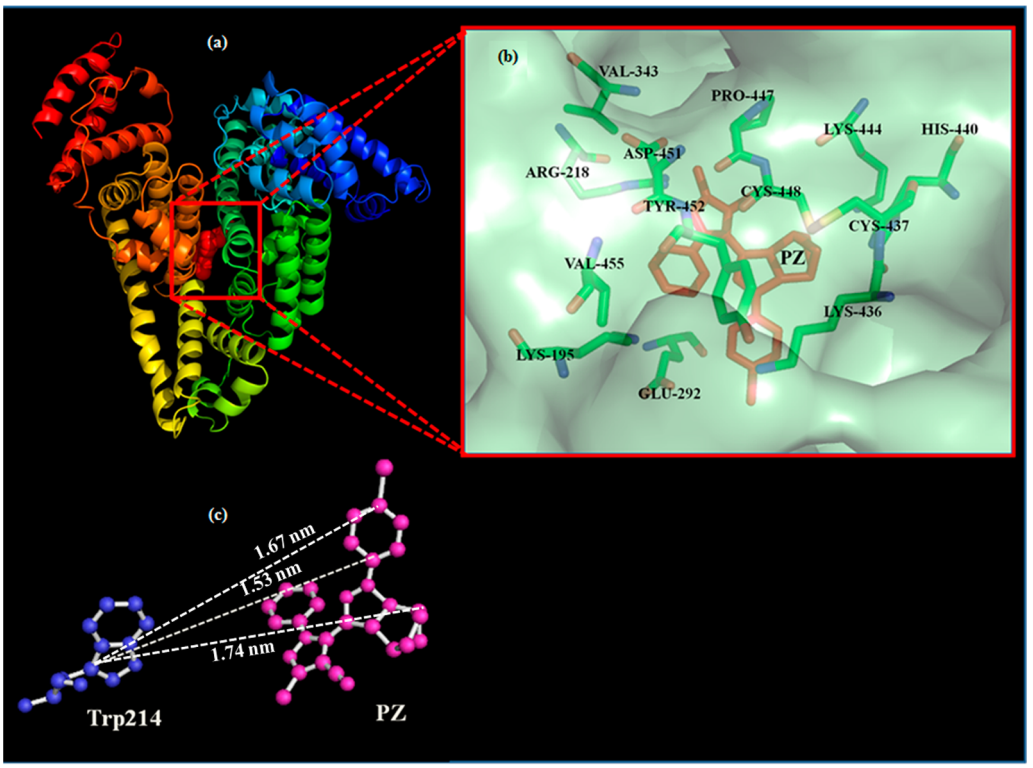

Figure 1. (a) Minimum-energy conformation of binding of PZ inside the scaffold of IIA subdomain HSA (PDB ID: 1AO6) as suggested by the molecular docking study. (b) A close view of the amino acid residues in the immediate vicinity of PZ. (c) Distances between Trp214 and PZ obtained from molecular docking study.

(d). Acrylamide Quenching. Acrylamide was used to quench the Trp214 fluorescence in HSA at various temperatures. A volume of 2.0 mL of a 10 μM HSA solution was titrated with varying concentrations (0−10 mM) of acrylamide in the buffer solution. The samples were excited at 295 nm, and the corresponding emissions were collected from 305 to 500 nm with an integration time of 0.1 s. The Stern−Volmer quenching constants in the presence of acrylamide (K_{SV}^{A}) were then calculated.

(e). Anisotropy Measurements. Steady-state anisotropy (r) can be defined by the following equation.

$$r = (I_{VV} - GI_{VH})/(I_{VV} + 2GI_{VH}) \quad (1)$$

where I_{VV} is the fluorescence intensity when both the excitation and emission polarizers are oriented vertically, and I_{VH} is the fluorescence intensity when the excitation polarizer is vertically and the emission polarizer is horizontally oriented. The G factor is given by

$$G = I_{HV}/I_{HH} \quad (2)$$

where I_{HV} is the fluorescence intensity with a horizontal excitation polarizer and a vertical emission polarizer, whereas I_{HH} is the fluorescence intensity with both the excitation and emission polarizers oriented horizontally.

(f). Atomic Force Microscopy. Atomic force microscopy (AFM) images were obtained from Agilent 5500 instrument. Mica sheets were used to prepare thin film of the samples prior to image scanning in noncontact AFM mode. The protein samples were left for about 0.5 h to air-dry and the AFM imaging was performed after the solvent was evaporated completely.

(g). Molecular Docking. The three-dimensional structure of the protein was obtained from Protein Data Bank with PDB code: 1AO6.[43] The PDB file corresponding to the structure of PZ was obtained from ChemDraw software package and saved in a compatible file format to be read in AutoDock4.2[14] software program. Blind docking study was performed to obtain the ligand (PZ)−protein (HSA) energy minimized docked conformation by AutoDock4.2 software program which uses the Lamarckian genetic algorithm (LGA).[14−17] During the docking study, all water molecules were removed and hydrogen atoms were added followed by computing Gasteiger charges, as required in LGA. The docking parameters used were as follows: grid size 126, 126, and 126 Å along the X, Y, and Z axes having 0.403 Å grid spacing. The center of the grid box was fixed at x,y,z = 29.551, 31.855, 23.559. The parameters corresponding to maximum number of energy evaluations, maximum number of generations, and GA crossover mode were fixed at 250 000, 27 000, and two points, respectively. The minimum binding energy conformer was searched out of 10 different conformers for the docking simulation and the resultant one was used for further analysis. The presented stereo view of the docked conformations has been prepared in PyMOL.[44]

RESULTS AND DISCUSSION

(a). Molecular Docking. Molecular docking has been employed to understand the interaction of PZ with HSA. Docking study suggests that the most favorable binding site of the probe is located inside a hydrophobic cavity of subdomain IIA or Sudlow site-I, near Trp214 amino acid residue of HSA (Figure 1a). The hydrophobic, electrostatic, and hydrogen bonding interactions play a major role for the binding and stabilization of PZ to the hydrophobic cavity of subdomain IIA

dx.doi.org/10.1021/jp5030944 | J. Phys. Chem. B XXXX, XXX, XXX−XXX

of HSA. The residues in the immediate vicinity of PZ in its binding pocket are Arg218, Lys195, Val343, Tyr452, and Asp451, Glu292, Lys436 and His440 (Figure 1b). Hydrophobic interactions of the nearby protein residues, Val and Ala, with PZ facilitate the anchoring of the nonpolar probe inside the hydrophobic pocket, while the residues Arg, Glu, Gln, Lys, Tyr, and Asp make polar contacts with the probe PZ in the HSA–PZ complex. It is also noticed that PZ binds in the close vicinity of Trp214 and the average distance between the two residues has been estimated to vary between 1.53 and 1.74 nm (Figure 1c). The binding of this bioactive molecule inside the protein scaffolds is rather strong and spontaneous and is characterized by a free energy of binding of -8.48 kcal mol^{-1}.

(b). Steady-State Fluorescence Spectroscopy. In aqueous buffer solution, PZ exhibits an absorption band peaked at 395 nm and has an emission peak at around 494 nm. These absorption and emission values are in excellent agreement with those reported in literature,[39] which corroborate the purity of the synthesized fluorophore. Upon incorporation inside the protein matrix (in the vicinity of Trp214, Sudlow's site: I), the absorption profile of PZ still remains the same (inset of Figure 2), whereas the emission

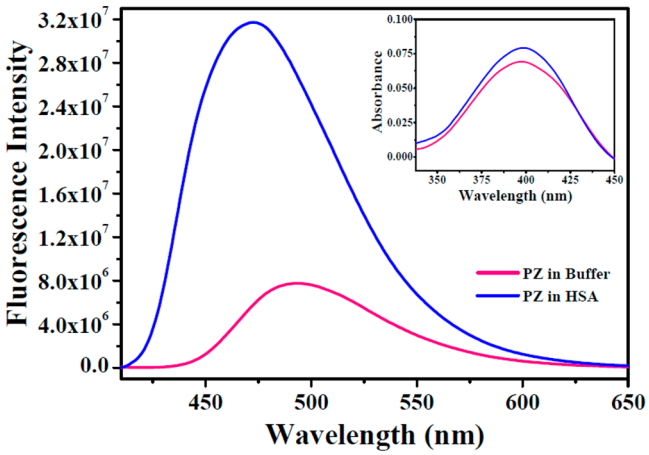

Figure 2. Steady-state fluorescence spectra of PZ in buffer and the presence of HSA. The inset represents the absorption spectra of PZ in buffer and the presence of HSA.

profile undergoes a drastic change. The fluorescence intensity increases by about 4 times and peaked at 474 nm thereby undergoing a blue-shift of about 20 nm (Figure 2) at 22 °C when excited at 395 nm. This enhancement in fluorescence intensity along with the 20 nm blue shift is a clear signature that PZ now experiences a more constrained hydrophobic environment as compared to the bulk. As the main objective of the present study was to elucidate the effect of temperature on the conformational dynamics of HSA, we have monitored the steady-state emission properties of both Trp214 and PZ as a function of temperature. Figure 3 represents the emission profiles of Trp214 and PZ at various temperatures and from the figure it is evident that the protein undergoes thermal denaturation and hence both the emission intensities of Trp214 and PZ decrease with rise in temperature except for 70 °C. As stated earlier, HSA has two melting temperatures (56 and 62 °C), and it would be very interesting to probe the structural changes the protein undergoes in the immediate vicinity of these temperatures. From 22 to 56 °C, the emission maxima for both Trp214 and PZ remains unchanged, centered

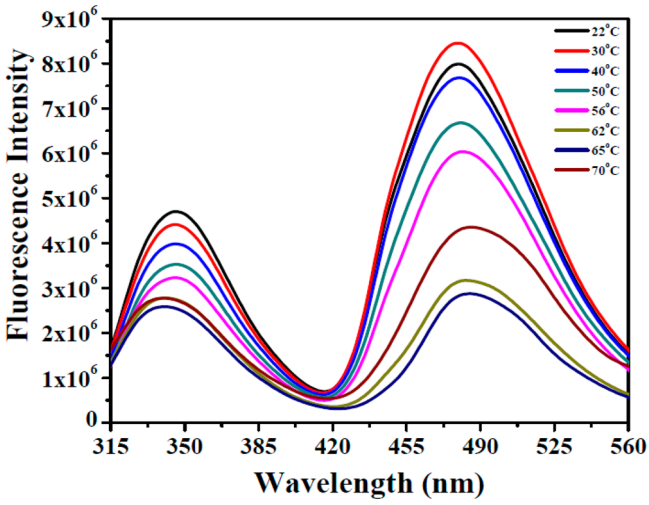

Figure 3. Steady-state fluorescence spectra of Trp214 in the presence of PZ at various temperatures as marked in the figure.

at 346 ± 1 and 480 ± 1 nm, respectively, when excited at 295 nm. This proves that the microenvironments of both the fluorophores remain the same within this temperature domain. On further increasing of temperature to 70 °C, contrary to our expectations, the Trp214 undergoes a blue shift of 6 nm and the peak is now centered at 340 nm. This blue shift in emission maxima signifies that, although the protein is undergoing thermal denaturation, upon increase of temperature, Trp214 gets more buried inside the hydrophobic scaffolds of the protein. This burial of Trp214 and the associated blue shift has been supported by our acrylamide quenching data (please see section Acrylamide Quenching for details). In a very seminal work, Pal and co-workers[37] have shown that the protein HSA loses a substantial portion of its helical content with a rise in temperature. Using temperature-dependent CD studies, they have observed that the α-helical content of the protein decreases from 65% at 20 °C to 38% at 70 °C and that the decrement of helicity is very rapid beyond 55 °C.[37] Since CD studies monitor the global structural changes the protein undergoes while intrinsic fluorescence experiments probe the immediate vicinity of the Trp214 amino acid residue, it may not be possible to draw a direct correlation between these two techniques. Our emission data of Trp214 is in excellent agreement with these observations; the Trp214 amino acid residue starts exhibiting a blue shift beyond 56 °C exemplifying the fact the microenvironment in and around the amino acid residue starts getting affected from this particular temperature. It must be mentioned here that the fluorescence intensity of Trp214 increases as the temperature is increased from 65 to 70 °C contrary to what was observed for other temperatures. This enhancement in fluorescence intensity can be ascribed to the formation of fibrils at very high temperatures (please see Atomic Force Microscopy section for details) which make the protein experience a more constrained environment.

The other fluorophore, PZ exhibits almost similar trend in fluorescence intensity except for the fact that there is a red shift of around 6 nm when the temperature is increased beyond 56 °C. This red shift in emission maxima suggests that the probe experiences a more hydrophilic environment beyond 56 °C and is most likely due to the loss of secondary structures[37,38] of the protein at elevated temperatures. Here also, there is a rise in fluorescence intensity beyond 65 °C, signifying that the fibril

dx.doi.org/10.1021/jp5030944 | J. Phys. Chem. B XXXX, XXX, XXX–XXX

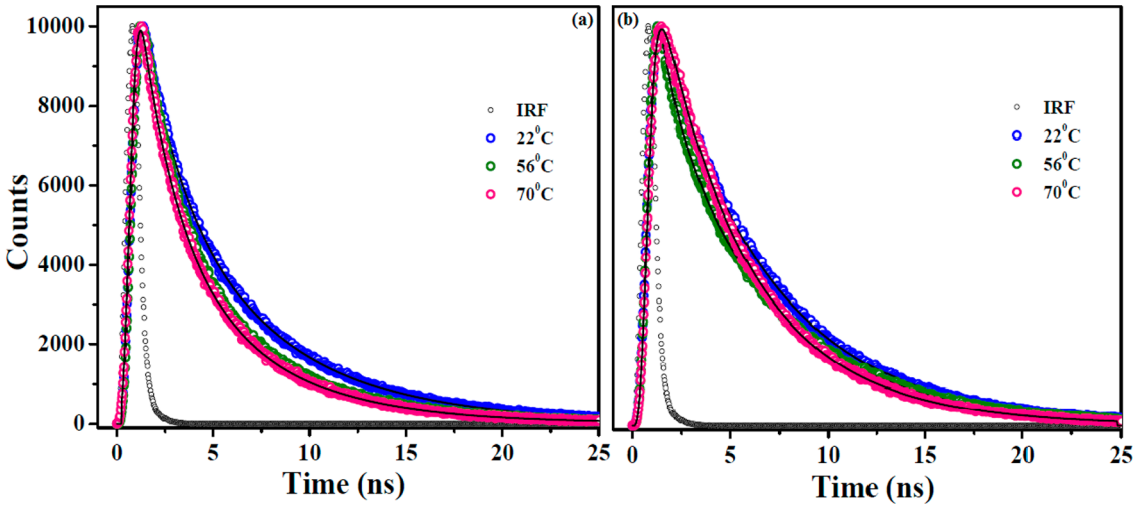

Figure 4. Fluorescence lifetime decays of (a) Trp214 and (b) PZ at 22, 56, and 70 °C. The IRF refers to the Instrument Response Function, i.e., the contribution from the laser diode which was deconvulated during fitting.

Table 1. Fluorescence Lifetime Parameters of Trp214 and PZ in the Presence of PZ

	Trp214						PZ					
temperature (°C)	a_1	τ_1 (ns)	a_2	τ_2 (ns)	$\langle\tau\rangle$ (ns)[a]	χ^{2b}	a_1	τ_1 (ns)	a_2	τ_2 (ns)	$\langle\tau\rangle$ (ns)[a]	χ^{2b}
22	17.73	2.01	82.27	6.08	5.36	1.05	4.35	2.64	95.65	5.88	5.75	1.10
30	20.88	2.12	79.12	5.93	5.15	1.03	5.8	2.61	94.2	5.95	5.75	1.09
40	22.91	2.11	77.09	5.73	4.90	1.05	4.08	1.54	95.92	5.88	5.70	1.07
50	25.08	2.08	74.92	5.8	4.72	1.08	8.07	1.09	91.93	5.87	5.48	1.16
56	25.37	1.80	74.63	5.29	4.40	1.07	6.28	1.06	93.78	5.80	5.50	1.06
62	26.81	1.82	73.11	5.17	4.26	1.0	14.93	3.62	85.07	5.84	5.50	1.12
65	26.64	1.75	73.36	5.11	4.21	1.15	30.47	3.68	69.53	5.93	5.24	1.05
70	28.64	1.87	71.36	5.20	4.14	1.11	45.68	3.70	54.32	6.06	4.98	1.0

[a]$\langle\tau\rangle = (a_1\tau_1 + a_2\tau_2)/100/$; ±5%. [b]The magnitude of χ^2 denotes the goodness of the fit.

formation encompasses a major section of the protein, which renders the PZ molecules to experience a more constrained environment. To see the effect of temperature on HSA in the absence of PZ, we have plotted the various emission profiles of Trp214 in Supporting Information Figure SI-2. Also, when PZ was exclusively monitored using an excitation wavelength of 395 nm (Supporting Information Figure SI-3), the same trend in the variation of emission spectra was obtained as encountered using an excitation wavelength of 295 nm.

(c). Time-Resolved Fluorescence Spectroscopy. Temperature induced protein conformational dynamics has been studied using time-resolved fluorescence spectroscopy. For lifetime measurements, samples were excited at 295 and 375 nm using a picosecond diode laser for monitoring Trp214 and PZ, respectively, at their respective emission maxima of the systems. Panels a and b of Figure 4 show the representative decay profiles of Trp214 and PZ at 22 °C, 56 and 70 °C temperatures, respectively. The values of decay parameters are summarized in Table 1. From Table 1, it is clear that with increasing temperature, the average lifetimes of both Trp214 and PZ decrease, but to different extents. The average lifetime of Trp214 in HSA (in the presence of PZ) is 5.36 ns at 22 °C. The decrement of lifetime is a manifestation of both quenching triggered by internal quencher moieties as well as due to temperature induced conformational transitions. The average lifetime of Trp214 decreases from 5.36 to 4.40 ns corresponding to a rise in temperature from 22 to 56 °C. The decrement of lifetime with increasing temperature is attributed to the structural deformation of HSA with marginal changes of microenvironment in and around Trp214. Beyond 56 °C, there is small decrement of lifetime (4.14 ns in at 70 °C). As 56 and 62 °C are the two melting temperatures of HSA, beyond 56 °C, HSA starts to unfold rapidly. But at same time, from the steady-state measurements, we have seen that a 6 nm blue shift of Trp214 occurs which implies that the microenvironment of Trp214 is more rigid as compared to its native state. Beyond 56 °C, there is a competition between (i) protein starting to unfold rapidly, thereby decreasing both the fluorescence intensity and lifetime; and (ii) Trp214 experiencing a more rigid environment, thereby increasing the fluorescence intensity. This interplay between the burial of Trp214 and thermal unfolding results in an overall decrement of the average lifetime of Trp214, but the magnitude of such a decrement is far lesser beyond the first melting temperature, 56 °C.

PZ binds to a region which is in the close vicinity to Trp214 (please refer to the Molecular Docking section for details); hence, it can be considered that temperature induced morphological changes of HSA affects the fluorescence lifetime of PZ in an manner very similar to that of Trp214. From Table 1 it is clear that up to 56 °C, PZ also follows the same trend as Trp214 (the average lifetime of PZ decreases 5.75 to 5.50 ns on increasing the temperature from 22 to 56 °C). Beyond 56 °C, the average lifetime of PZ further decreases to 4.98 ns at 70 °C. Here also, the thermal denaturation renders PZ to experience a more polar environment as compared to 56 °C (please refer to

dx.doi.org/10.1021/jp5030944 | J. Phys. Chem. B XXXX, XXX, XXX−XXX

the 6 nm red shift in the emission maxima). However, the fibril formation accounts for a more constrained environment for PZ resulting in an overall decrement of the average lifetime beyond 56 °C.

(d). Binding Interactions of PZ with HSA. As mentioned earlier, molecular docking experiments revealed that the binding of PZ to HSA is spontaneous and is characterized by a free energy of binding of −8.48 kcal mol^{-1}. This prompted us to estimate the nature of binding using our steady-state and time-resolved data. To this effect, we have monitored the change in fluorescence intensities of Trp214 at room temperature (22 °C) with varying concentrations of PZ which quenches the emission of Trp214. Fluorescence quenching can be best monitored by analyzing the Stern−Volmer equation:[21,22,42]

$$F_o/F = 1 + K_{SV}[Q] = 1 + k_q\tau_0[Q] \quad (3)$$

In the above equation, F_0 and F are the fluorescence intensities of the fluorophore (Trp214 in HSA) in the absence and presence of quencher, respectively. [Q] is the quencher (PZ in the present case) concentration and K_{SV} is the Stern−Volmer quenching constant, k_q is the bimolecular quenching rate constant, and τ_0 is the average lifetime of fluorophore in absence of quencher. Also, from our steady-state results, we further estimated the binding constant (K) and the binding affinity (n) using a modified version of the Stern−Volmer equation:[21,22,42]

$$\log[(F_0 - F)/F] = \log K + n \log[Q] \quad (4)$$

The associated thermodynamics of binding can be estimated by measuring the free energy of binding ($\Delta G^0_{Binding}$) given by

$$\Delta G^0_{Binding} = -2.303RT \log K \quad (5)$$

The quenching of fluorescence is known to occur by two processes, namely collisional (dynamic) quenching and/or formation of a complex between the quencher and fluorophore (static quenching).[42] The linear type of Stern−Volmer plot (figure not shown) reveals that only one type of quenching is operational.[42] As seen from eq 4, a plot of $\log[(F_0 - F)/F]$ against log[Q] is expected to be linear and from the slope and intercept, n and K can be estimated (Figure SI-4a, SI Table-1). To support the mechanistic pathway of the addition of PZ to HSA, we have used the average lifetime values instead of fluorescence intensities in analogy with eq 4 as

$$\log[(\langle\tau\rangle_0 - \langle\tau\rangle)/\langle\tau\rangle] = \log K + n \log[Q] \quad (6)$$

where, $\langle\tau\rangle_0$ and $\langle\tau\rangle$ represent the average lifetime values of HSA in the absence and presence of PZ. A plot of $\log[(\langle\tau\rangle_0 - \langle\tau\rangle)/\langle\tau\rangle]$ against log[Q] is shown in Figure SI-4b. The K_{SV} values are indicative of the fact that PZ indeed quenches the fluorescence of Trp214 significantly and also the interaction between PZ and HSA is pretty strong as evident from the magnitudes of K. As seen from SI Table-1, all the parameters mentioned therein, obtained from steady-state and time-resolved measurements, are almost similar. The high values of the bimolecular rate constants ($k_q \sim 10^{12}$ s^{-1}, SI Table-1) are a clear signature of the fact that the interaction between PZ and HSA is diffusion controlled.[41] If the mechanism of quenching was through the formation of a complex, i.e., if static quenching was operational, then the lifetimes of the probe molecule would not have been affected by a large extent. Since the magnitudes of both K_{SV} and K obtained from steady-state (which monitors ground state phenomena) and time-resolved (which monitors excited-state phenomena) experiments are in excellent agreement with each other, we can rationally conclude that the mechanism of quenching is most likely collisional/diffusion controlled. Our observations are also in unison with those reported in the literature.[41] Also, the magnitudes of the free energy of binding as obtained from our spectroscopic data agree very well with that reported by our molecular docking studies. This further substantiates the correlation between these two methodologies and confirms the rationality of our computational results.

(e). Energy Transfer. Fluorescence resonance energy transfer (FRET) is a spectroscopic phenomenon, where energy is transferred from the excited state donor fluorophore to the ground state acceptor fluorophore via nonradiative long-range dipole−dipole interactions.[42] FRET can elucidate morphological changes or conformational dynamics of a biomacromolecule and hence can be used to estimate the distance between different domains where the donor and acceptor molecules are located. According to Förster nonradiative energy transfer theory,[42] the efficiency of energy transfer (E_{FRET}) depends upon the distance between the donor and the acceptor (r_0) and the critical energy transfer distance (R_0) as

$$E_{FRET} = \frac{R_0^6}{R_0^6 + r_0^6} \quad (7)$$

where the Förster distance, R_0, is the critical distance at which the energy transfer efficiency is 50%. The magnitude of R_0 can be estimated by the following equation:

$$R_0^6 = 8.8 \times 10^{-25}\kappa^2 N^{-4}\phi J \quad (8)$$

where κ^2 is the spatial orientation factor related to orientation in space of the transition dipoles of the donor and acceptor, N is the average refractive index of the medium (here buffer), ϕ is the fluorescence quantum yield of the donor in the absence of acceptor, and J is the spectral overlap integral between the donor fluorescence emission spectrum and the acceptor absorption spectrum. The magnitude of the spectral overlap integral, J is given by

$$J = \frac{\Sigma F(\lambda)\varepsilon(\lambda)\lambda^4\Delta\lambda}{\Sigma F(\lambda)\Delta\lambda} \quad (9)$$

where $F(\lambda)$ is the fluorescence intensity of the donor at wavelength λ, and $\varepsilon(\lambda)$ is the molar absorption coefficient of the acceptor at that wavelength λ (expressed in M^{-1} cm^{-1}). Figure SI-5 represents the spectral overlap at 22 °C, between the donor (Trp214 in the present case) emission and the acceptor (PZ in the present case) absorption. From the extent of overlap, it is pretty evident that Trp214 and PZ form a very good FRET pair and hence can be used to monitor the temperature dependent conformational dynamics of HSA. From the extent of spectral overlap at various temperatures and by using eq 9, the J values for the Trp214-PZ FRET pair has been estimated to be 7.38×10^{-15}, 6.4×10^{-15}, and 6.45×10^{-15} at 22, 56, and 70 °C, respectively.

The efficiency of energy transfer (E_{FRET}) can be best studied from time-resolved measurements and the magnitude of E_{FRET} is given by[24,42,45−47]

$$E_{FRET} = 1 - \tau_{DA}/\tau_D \quad (10)$$

dx.doi.org/10.1021/jp5030944 | J. Phys. Chem. B XXXX, XXX, XXX−XXX

Table 2. Various Parameters Obtained from Steady-State and Time-Resolved Fluorescence Studies

	temperature (°C)							
	22	30	40	50	56	62	65	70
E_{FRET} (%)	4.2	4.6	4.1	3.6	8.7	10.12	10.9	13.2
Steady-State Anisotropy of PZ	0.17	0.16	0.17	0.15	0.17	0.23	0.24	0.33
Rotational Relaxation Time of PZ (ns)	29.7	27.5	26.2	38.6	32.3	51.2	54.3	85.6
K_{SV}^{A} (M^{-1})	10.5	8.9	10.7	7.7	6.9	5.0	4.6	-

where, τ_{DA} and τ_{D} are the lifetimes of the donor in the presence and absence of the acceptor, respectively. Using the values of average lifetimes of Trp214 in the absence (SI Table-2) and presence (Table 1) of PZ, the values of E_{FRET} have been estimated at various temperatures (Table 2).

Putting the values of $\kappa^2 = 2/3$, $N = 1.36$, and $\phi = 0.15$, and by using eqs 7−10, the critical energy transfer distance (R_0) and the distance between the donor and the acceptor (r_0) has been calculated and the results are summarized in Table 3. The

Table 3. FRET Parameters at Different Temperatures

temperature (°C)	E_{FRET} (%)	R_0 (nm)	r_0 (nm)
22	4.2	2.24	3.78
56	8.7	2.20	3.24
70	13.2	2.19	2.98

distance between Trp214 and PZ has been estimated to be 3.78 nm at 22 °C. With increasing temperature up to 50 °C, E_{FRET} values exhibit minor variations with a rise in temperature (Table 2, Figure 5). As stated earlier, the first melting

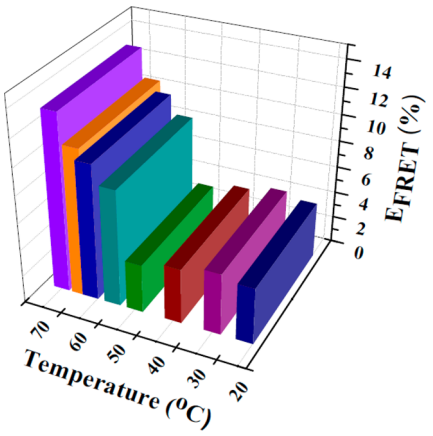

Figure 5. Plot of efficiency of energy transfer (E_{FRET}) from Trp214 (donor) to PZ (acceptor) as a function of temperature from 22 to 70 °C.

temperature of HSA is 56 °C and our E_{FRET} data also supports this fact. At such a temperature, the magnitude of E_{FRET} shows a rapid rise (Table 2); Trp214 which is deep-seated inside the protein scaffolds becomes labile, and consequently, the distance between Trp214 and PZ becomes lesser (Table 3). On further increasing the temperature up to 70 °C, the magnitude of E_{FRET} increases to 13.2% and the distance between the donor and the acceptor has been estimated to be around 2.98 nm. At such elevated temperatures, HSA is known to form fibrils,[48,49] and hence, in all probabilities, this aggregation behavior results in an enhancement of E_{FRET} and subsequently brings the Trp214 and PZ fluorophores closer to each other. Thus, our temperature-dependent monitoring of E_{FRET} gave us a clearer picture of the conformational changes that HSA undergoes with the variation of temperature.

(f). Steady-State and Time-Resolved Anisotropy of PZ. Fluorescence anisotropy measurements can be used to quantify protein denaturation which usually results in an increased flexibility of the different domains present within the biomolecule.[42] Hence, temperature induced conformational dynamics of protein can be well characterized by anisotropy measurements. In a more constrained environment, the motion of a fluorophore is restricted which in turns increases its anisotropy values.

In the present study, we have used both the steady-state and time-resolved anisotropy to monitor the effect of temperature on the rotational motions of PZ. Figure 6 demonstrates a

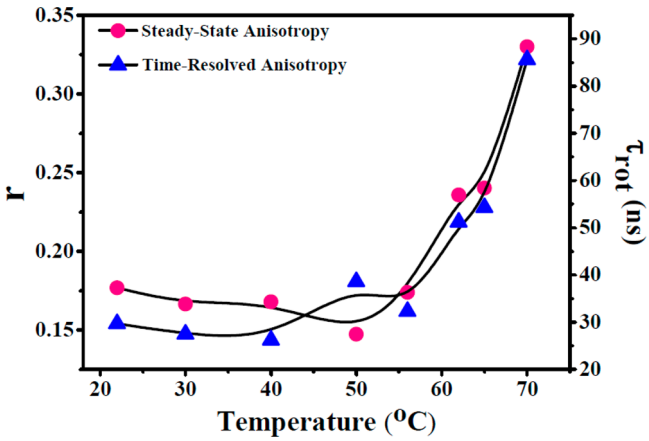

Figure 6. Simultaneous plot of the steady-state and time-resolved anisotropy of PZ in HSA.

simultaneous plot of the variation of steady-state and time-resolved anisotropies of PZ with temperature. As seen from the figure, both the steady-state and time-resolved anisotropy values complement each other very well. The microenvironment until the first melting point of HSA (56 °C) as experienced by PZ is almost constant and this observation is in excellent agreement with our steady-state results. Beyond this particular temperature, both the steady-state and time-resolved anisotropy values increase rapidly, signifying that the process of aggregation may get initiated beyond 56 °C (Table 2). As shown by Takeda and co-workers,[38] the rise in β-sheet content at elevated temperatures is also well supported by our anisotropy measurements; the maximum value is also obtained at 70 °C. Using DLS experiments, Pal and co-workers[37] have concluded that the hydrodynamic radius (d_H) of HSA undergoes a 4-fold increment when the temperature is raided from 25 to 70 °C. They further established that d_H remains almost constant until 60 °C, beyond which it rises very sharply.[37] Our steady-state and time-resolved anisotropy values not only agree very well with these data but also support the

dx.doi.org/10.1021/jp5030944 | J. Phys. Chem. B XXXX, XXX, XXX−XXX

fact that the protein undergoes conformational changes mainly beyond its first melting point temperature, 56 °C.

(g). Acrylamide Quenching. Acrylamide, which is a small and neutral molecule, having a diffusion rate similar to water, has been widely used to probe the tryptophan accessibility of proteins.[50−52] The Stern−Volmer quenching constant of HSA in the presence of acrylamide (K_{SV}^{A}) has been estimated to be 10.5 M^{-1} 22 °C which decreases to 4.6 M^{-1} at 65 °C (Table 2). At temperatures less than 56 °C, Trp214 experiences an environment which is more or less uniform and this observation has been well-supported by our steady-state spectroscopic data. Beyond the first melting point of HSA (56 °C), we have seen that the Trp214 undergoes a 6 nm blue shift signifying the fact that it gets buried inside the protein scaffolds. This hypsochromic shift in emission maxima of Trp214 has been correlated with our acrylamide quenching studies. The K_{SV}^{A} values show a sharp decrement beyond 56 °C which can be attributed to the fact that the Trp214 becomes less accessible toward the acrylamide. The variation of emission maxima of Trp214 with temperature and its direct correlation with the K_{SV}^{A} values are depicted in Figure 7. From the figure, it

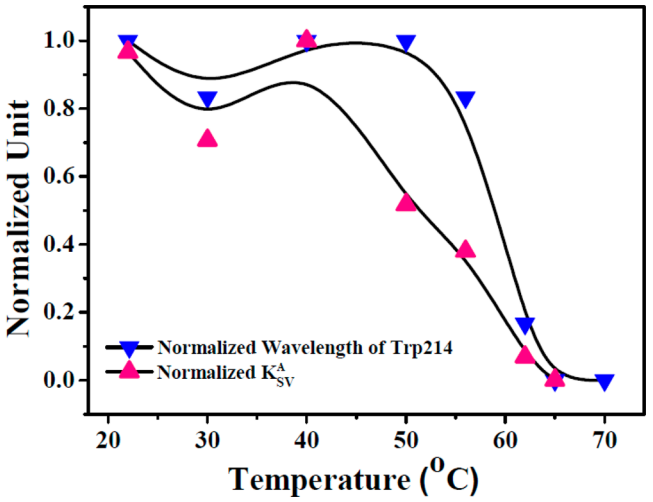

Figure 7. Simultaneous normalized plot of acrylamide quenching constant (K_{SV}^{A}) of Trp214 in HSA and wavelength shift upon increasing temperature from 22 to 70 °C.

is pretty evident that at higher temperatures when Trp214 gets buried and experiences a more hydrophobic environment, the K_{SV}^{A} values decrease thereby accounting for the 6 nm blue shift of Trp214.

(h). Atomic Force Microscopy. Morphological transitions of HSA were investigated as a function of temperature using AFM that provided us with insights into the topography of the nanoscale structural assemblies. For this purpose, we have compared the AFM micrographs of HSA at 56 and 70 °C with that recorded at 22 °C which served as a control. From Figure 8a, it is evident that HSA displays no visible pattern at 22 °C. However, when the first melting temperature is reached, the protein starts to form aggregates and this is clearly seen form Figure 8b where spherical aggregates of a varied distribution can be seen. At 70 °C, the AFM micrograph displays the existence of fibrils (Figure 8c) which is in very good agreement with our other spectroscopic data. Although the existence of fibrils is not absolute at this elevated temperature as it also has some spherical aggregates, the constrained environment as experienced by the fluorophores at 70 °C can thus be attributed to the formation of such fibrils as seen from the AFM data. The reason for the fibril formation can be attributed to the loss of α-helical content of the protein thereby resulting in a concomitant rise in the β-sheet structure. Our observations are in excellent agreement to the previous studies on serum albumins where fibril formation at elevated temperatures has been documented owing to the formation of β-sheets.[38,53]

CONCLUSIONS

In this present work, we have reported the effect of temperature on the conformational dynamics of the protein, HSA. Using steady-state and time-resolved spectroscopic approaches, we have conclusively proved that HSA undergoes morphological changes mainly beyond its first melting temperature, 56 °C. Time-resolved FRET has been employed to have an estimate of the distance between the donor (Trp214) and acceptor (PZ) which has been found to vary with temperature. Our FRET results have been supported by molecular docking studies, which prove that the binding site of the synthesized bioactive molecule, PZ, is indeed very close to the Trp214 amino acid residue. The temperature induced denaturation of the protein has been extensively studied using the intrinsic fluorescence of Trp214 amino acid residue, and most interestingly, although undergoing thermal denaturation, the Trp214 residue gets buried inside the protein scaffolds, which is corroborated by its 6 nm blue shift. This behavior of the Trp214 residue has been well supported by our acrylamide quenching studies as well. Using Stern−Volmer and modified Stern−Volmer equations, we have proved that the principal mechanism of quenching of Trp214 by PZ is dynamic in nature. Finally, we have concluded that at elevated temperatures (70 °C), the protein undergoes self-assembly to form fibrillar structures, which has been correlated to the temperature dependent AFM micrographs. This morphological transition to form fibrils has been ascribed to the loss of α-helical content of the protein which in turn gives rise to β-sheet structures.

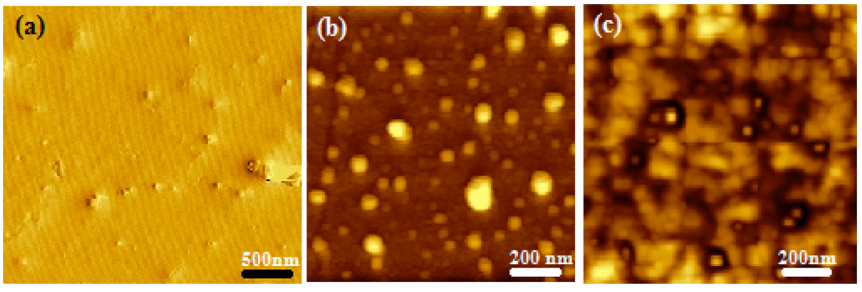

Figure 8. AFM micrographs of HSA samples at (a) 22, (b) 56, and (c) 70 °C.

dx.doi.org/10.1021/jp5030944 | J. Phys. Chem. B XXXX, XXX, XXX−XXX

■ ASSOCIATED CONTENT

Supporting Information

Details of the spectroscopic characterization of PZ by NMR and HRMS, emission profiles of Trp214 and PZ, steady-state and time-resolved quenching parameters and lifetime parameters of HSA in the absence of PZ as a function of temperature. This material is available free of charge via the Internet at http://pubs.acs.org.

■ AUTHOR INFORMATION

Corresponding Authors

*E-mail: mk@iiserb.ac.in.

*E-mail: saptarshi@iiserb.ac.

Notes

The authors declare no competing financial interest.

■ ACKNOWLEDGMENTS

We sincerely thank Department of Science & Technology, New Delhi, India, for the DST-Fast Track Scheme (No.: SR/FT/CS-19/2011) Science & Engineering Research Board (SERB) for financial support. N.K.D., A.P.K., and S.G. thank UGC, Govt. of India and N.G., U.A., and V.K.T. thank CSIR, Govt. of India for providing fellowships. S.M. thanks Dr. Bijan Kumar Paul for helping us with the molecular docking studies.

■ REFERENCES

(1) Peters, T. *All about Albumins: Biochemistry, Genetics, and Medical Applications*; Academic Press: San Diego, CA, 1996.

(2) Peters, T., Jr. Serum Albumin. *Adv. Protein Chem.* **1985**, *37*, 161−245.

(3) Sudlow, G.; Birkett, D. J.; Wade, D. N. The Characterization of Two Specific Drug Binding Sites on Human Serum Albumin. *Mol. Pharmacol.* **1975**, *11*, 824−832.

(4) Bertucci, C.; Dominici, E. Reversible and Covalent Binding of Drugs to Human Serum Albumin: Methodological Approaches and Physiological Relevance. *Curr. Med. Chem.* **2002**, *9*, 1463−1481.

(5) Kragh-Hansen, U.; Chuang, V. T.; Otagiri, M. Practical Aspects of the Ligand-Binding and Enzymatic Properties of Human Serum Albumin. *Biol. Pharm. Bull.* **2002**, *25*, 695−704.

(6) Sakurai, Y.; Ma, S. F.; Watanabe, H.; Yamaotsu, N.; Hirono, S.; Kurono, Y.; Kragh-Hansen, U.; Otagiri, M. Esterase-like Activity of Serum Albumin: Characterization of its Structural Chemistry Using p-Nitrophenyl Esters as Substrates. *Pharm. Res.* **2004**, *21*, 285−292.

(7) Yang, F.; Bian, C.; Zhu, L.; Zhao, G.; Huang, Z.; Huang, M. Effect of Human Serum Albumin on Drug Metabolism: Structural Evidence of Esterase Activity of Human Serum Albumin. *J. Struct. Biol.* **2007**, *157*, 348−355.

(8) Ascenzi, P.; Fasano, M. Allostery in a Monomeric Protein: The Case of Human Serum Albumin. *Biophys. Chem.* **2010**, *148*, 16−22.

(9) He, X. M.; Carter, D. C. Atomic Structure and Chemistry of Human Serum Albumin. *Nature* **1992**, *358*, 209−215.

(10) Narazaki, R.; Maruyama, T.; Otagiri, M. Probing the Cysteine 34 Residue in Human Serum Albumin Using Fluorescence Techniques. *Biochim. Biophys. Acta* **1997**, *1338*, 275−281.

(11) Anand, U.; Mukherjee, S. Binding, Unfolding and Refolding Dynamics of Serum Albumin. *Biochem. Biophys. Acta, Gen. Subj.* **2013**, *1830*, 5394−5404.

(12) De, D.; Kaur, H.; Datta, A. Unusual Binding of a Potential Biomarker with Human Serum Albumin. *Chem.—Asian J.* **2013**, *8*, 728−735.

(13) Trynda-Lemiesz, L. Paclitaxel−HSA Interaction. Binding Sites on HSA Molecule. *Bioorg. Med. Chem.* **2004**, *12*, 3269−3275.

(14) Morris, G. M.; Goodesell, D. S.; Halliday, R. S.; Huey, R.; Hart, W. E.; Bellew, R. K.; Olson, A. J. Automated Docking Using a Lamarckian Genetic Algorithm and an Empirical Binding Free Energy Function. *J. Comput. Chem.* **1999**, *19*, 1639−1662.

(15) Granum, D. M.; Vyas, S.; Sambasivarao, S. V.; Maupin, C. M. Computational Evaluations of Charge Coupling and Hydrogen Bonding in the Active Site of a Family 7 Cellobiohydrolase. *J. Phys. Chem. B* **2014**, *118*, 434−448.

(16) Bolel, P.; Datta, S.; Mahapatra, N.; Halder, M. Exploration of pH-Dependent Behavior of the Anion Receptor Pocket of Subdomain IIA of HSA: Determination of Effective Pocket Charge Using the Debye−Hückel Limiting Law. *J. Phys. Chem. B* **2014**, *118*, 26−36.

(17) Liu, Y.; Ma, L.; Chen, W.; Park, H.; Ke, Z.; Wang, B. Binding Mechanism and Synergetic Effects of Xanthone Derivatives as Noncompetitive α-Glucosidase Inhibitors: A Theoretical and Experimental Study. *J. Phys. Chem. B* **2013**, *117*, 13464−13471.

(18) Shaw, B. F.; Schneider, G. F.; Arthanari, H.; Narovlyansky, M.; Moustakas, D. T.; Durazo, A.; Wagner, G.; Whitesides, G. M. Complexes of Native Ubiquitin and Dodecyl Sulfate Illustrate the Nature of Hydrophobic and Electrostatic Interactions in the Binding of Proteins and Surfactants. *J. Am. Chem. Soc.* **2011**, *133*, 17681−17695.

(19) Mukherjee, S.; Sen, P.; Halder, A.; Sen, S.; Dutta, P.; Bhattacharyya, K. Solvation Dynamics in a Protein−Surfactant Aggregate. TNS in HSA−SDS. *Chem. Phys. Lett.* **2003**, *379*, 471−478.

(20) Mandal, U.; Ghosh, S.; Mitra, G.; Adhikary, A.; Dey, S.; Bhattacharyya, K. A Femtosecond Study of the Interaction of Human Serum Albumin with a Surfactant (SDS). *Chem.—Asian J.* **2008**, *3*, 1430−1434.

(21) Anand, U.; Jash, C.; Mukherjee, S. Spectroscopic Probing of the Microenvironment in a Protein-Surfactant Assembly. *J. Phys. Chem. B* **2010**, *114*, 15839−15845.

(22) Anand, U.; Jash, C.; Boddepalli, R. K.; Shrivastava, A.; Mukherjee, S. Exploring the Mechanism of Fluorescence Quenching in Proteins Induced by Tetracycline. *J. Phys. Chem. B* **2011**, *115*, 6312−6320.

(23) Takeda, K.; Moriyama, Y. Comment on the Misunderstanding of the BSA−SDS Complex Model: Concern about Publications of an Impractical Model. *J. Phys. Chem. B* **2007**, *111*, 1244−1244.

(24) Patel, S.; Datta, A. Steady-State and Time-Resolved Fluorescence Investigation of the Specific Binding of Two Chlorin Derivatives with Human Serum Albumin. *J. Phys. Chem. B* **2007**, *111*, 10557−10562.

(25) Krishnakumar, S. S.; Panda, D. Spatial Relationship between the Prodan Site, Trp-214, and Cys-34 Residues in Human Serum Albumin and Loss of Structure Through Incremental Unfolding. *Biochemistry* **2002**, *41*, 7443−7452.

(26) Santra, M. K.; Banerjee, A.; Rahaman, O.; Panda, D. Unfolding Pathways of Human Serum Albumin: Evidence for Sequential Unfolding and Folding of its Three Domains. *Int. J. Biol. Macromol.* **2005**, *37*, 200−204.

(27) Chakraborty, A.; Seth, D.; Setua, P.; Sarkar, N. Photoinduced Electron Transfer in a Protein-Surfactant Complex: Probing the Interaction of SDS with BSA. *J. Phys. Chem. B* **2006**, *110*, 16607−16617.

(28) Thakur, G.; Jiang, K.; Lee, D.; Prashanthi, K.; Kim, S.; Thundat, T. Investigation of pH-Induced Protein Conformation Changes by Nanomechanical Deflection. *Langmuir* **2014**, *30*, 2109−2116.

(29) Bharmoria, P.; Rao, K. S.; Trivedi, T. J.; Kumar, A. Biamphiphilic Ionic Liquid Induced Folding Alterations in the Structure of Bovine Serum Albumin in Aqueous Medium. *J. Phys. Chem. B* **2014**, *118*, 115−124.

(30) Baler, K.; Martin, O. A.; Carignano, M. A.; Ameer, G. A.; Vila, J. A.; Szleifer, I. Electrostatic Unfolding and Interactions of Albumin Driven by pH Changes: A Molecular Dynamics Study. *J. Phys. Chem. B* **2014**, *118*, 921−930.

(31) Leggio, C.; Galantini, L.; Konarev, P. V.; Pavel, N. V. Urea Induced Denaturation Process on Defatted Human Serum Albumin and in the Presence of Palmitic Acid. *J. Phys. Chem. B* **2009**, *113*, 12590−12602.

(32) Heller, W. T. Comparison of the Thermal Denaturing of Human Serum Albumin in the Presence of Guanidine Hydrochloride

and 1-Butyl-3-Methylimidazolium Ionic Liquids. *J. Phys. Chem. B* **2013**, *117*, 2378−2383.
(33) Fu, L.; Villette, S.; Petoud, S.; Fernandez-Alonso, F.; Saboungi, M. H/D Isotope Effects in Protein Thermal Denaturation: The Case of Bovine Serum Albumin. *J. Phys. Chem. B* **2011**, *115*, 1881−1888.
(34) Hédoux, A.; Willart, J.; Paccou, L.; Guinet, Y.; Affouard, F.; Lerbret; Descamps, M. Thermostabilization Mechanism of Bovine Serum Albumin by Trehalose. *J. Phys. Chem. B* **2009**, *113*, 6119−6126.
(35) Flora, K.; Brennan, J. D.; Baker, G. A.; Doody, M. A.; Bright, F. V. Unfolding of Acrylodan-Labeled Human Serum Albumin Probed by Steady-State and Time-Resolved Fluorescence Methods. *Biophys. J.* **1998**, *75*, 1084−1096.
(36) Pico, G. A. Thermodynamic Features of the Thermal Unfolding of Human Serum Albumin. *Int. J. Biol. Macromol.* **1997**, *20*, 63−73.
(37) Mitra, R. K.; Sinha, S. S.; Pal, S. K. Hydration in Protein Folding: Thermal Unfolding/Refolding of Human Serum Albumin. *Langmuir* **2007**, *23*, 10224−10229.
(38) Takeda, K.; Wada, A.; Yamamoto, K.; Moriyama, Y.; Aoki, K. Conformational Change of Bovine Serum Albumin by Heat Treatment. *J. Protein Chem.* **1989**, *8*, 653−659.
(39) Chatterjee, S.; Banerjee, P.; Pramanik, S.; Mukherjee, A.; Mahalanabis, K. K.; Bhattacharya, S. C. Role of Homogeneous Solvents on Photophysics of 3-Pyrazolyl-2-Pyrazoline Derivative. *Chem. Phys. Lett.* **2007**, *440*, 313−320.
(40) Goodell, J. R.; Puig-Basagoiti, F.; Forshey, B. M.; Shi, P. Y.; Ferguson, D. M. Identification of Compounds with Anti-West Nile Virus Activity. *J. Med. Chem.* **2006**, *49*, 2127−2137.
(41) Banerjee, P.; Pramanik, S.; Sarkar, A.; Bhattacharya, S. C. Deciphering the Fluorescence Resonance Energy Transfer Signature of 3-Pyrazolyl 2-Pyrazoline in Transport Proteinous Environment. *J. Phys. Chem. B* **2009**, *113*, 11429−11436.
(42) Lakowicz, J. R. *Principles of Fluorescence Spectroscopy*; Kluwer Academic: New York, 1999.
(43) Sugio, S.; Kashima, A.; Mouchizuki, S.; Noda, M.; Kobayashi, K. Crystal Structure of Human Serum Albumin at 2.5 Å Resolution. *Protein Eng.* **1999**, *12*, 439−446.
(44) De Lano, W. L. *The PyMOL Molecular Graphics System*; De Lano Scientific: San Carlos, CA, 2002.
(45) Shaw, A. K.; Pal, S. K. Spectroscopic Studies on the Effect of Temperature on pH-Induced Folded States of Human Serum Albumin. *J. Photochem. Photobiol., B* **2008**, *90*, 69−77.
(46) Sahu, K.; Ghosh, S.; Mondal, S. K.; Ghosh, B. K.; Sen, P.; Roy, D.; Bhattacharyya, K. Ultrafast Fluorescence Resonance Energy Transfer in a Micelle. *J. Chem. Phys.* **2006**, *125*, 044714.
(47) Huang, F.; Lerner, E.; Sato, S.; Amir, D.; Hass, E.; Fresht, A. R. Time-Resolved Fluorescence Resonance Energy Transfer Study Shows a Compact Denatured State of the B Domain of Protein. *Biochemistry* **2009**, *48*, 3468−3476.
(48) Juarez, J.; Taboada, P.; Mosquera, V. Existence of Different Structural Intermediates on the Fibrillation Pathway of Human Serum Albumin. *Biophys. J.* **2009**, *96*, 2353−2370.
(49) Pandey, N. K.; Ghosh, S.; Dasgupta, S. Fibrillation in Human Serum Albumin is Enhanced in the Presence of Copper (II). *J. Phys. Chem. B* **2010**, *114*, 10228−10233.
(50) Eftink, M. R.; Ghiron, C. A. Exposure of Tryptophanyl Residues in Proteins. Quantitative Determination by Fluorescence Quenching Studies. *Biochemistry* **1976**, *15*, 672−680.
(51) Eftink, M. R.; Ghiron, C. A. Fluorescence Quenching of Indole and Model Micelle Systems. *J. Phys. Chem.* **1976**, *80*, 486−493.
(52) Merrill, A. R.; Palmer, L. R.; Szabo, A. G. Acrylamide Quenching of the Intrinsic Fluorescence of Tryptophan Residues Genetically Engineered into the Soluble Colicin E1 Channel Peptide. Structural Characterization of the Insertion-Competent State. *Biochemistry* **1993**, *32*, 6974−6981.
(53) Callaghan, P.; Martin, N. H. The Relation of the Rotatory Dispersion Behaviour of Human Serum Albumin to its Configuration. *Biochem. J.* **1962**, *83*, 144−151.